**Science Press**

ARTICLE

# Microstructure, Texture, and Mechanical Properties of Mg-Zn-Y-Nd-Zr Alloys

Wang Ziyi[1], Chen Xianhua[1,2], Shu Yankai[1], Li Jianbo[1], Yuan Yuan[1], Tan Jun[1], Pan Fusheng[1,2]

[1] College of Materials Science and Engineering, Chongqing University, Chongqing 400045, China; [2] National Engineering Research Center for Magnesium Alloys, Chongqing 400044, China

**Abstract:** The microstructure and mechanical properties of Mg-Zn-Y-Nd-Zr alloys were studied in this research. Results show that the added Nd element partially replaces the Y element in the W phase ($Mg_3Zn_3Y_2$), forming a new secondary phase $Mg_3Zn_3(Y, Nd)_2$. A typical bimodal structure consisting of fine equiaxed recrystallized grains and coarse elongated unrecrystallized grains can be observed in the alloy after thermal extrusion. The Nd addition promotes the dynamic recrystallization during hot extrusion. With increasing the Nd content, the dynamic recrystallization ratio is increased, and the overall texture strength of the as-extruded alloy is weakened. The addition of Nd element refines the grains and improves the mechanical properties of Mg-Zn-Y-Zr alloy. When 0.5wt% Nd is added, the mechanical properties of as-extruded alloy show a good combination of high strength and high plasticity: the yield strength is 362 MPa, the ultimate tensile strength is 404 MPa, and the elongation is 10.2%. After aging treatment, the tensile strength of the alloy is further improved, and the ultimate tensile strength of the alloy after peak aging treatment reaches 421 MPa. The high strength of the Mg-Zn-Y-Nd-Zr alloy is mainly attributed to ultrafine recrystallized grains and precipitation strengthening.

**Key words:** Mg-Zn-Y-Nd-Zr alloy; dynamic recrystallization; mechanical properties; texture

Magnesium alloys are lightweight metallic structural materials and attract much attention in electric, automotive, and aerospace industries[1,2]. Due to the low density of magnesium alloys, the improved fuel efficiency, reduced emission, and low cost can be achieved[3-5]. However, the magnesium alloys are not widely used in industrial fields, because their strength is inferior to that of the steel and aluminum alloys. Besides, the comprehensive properties of Mg alloys cannot meet the application requirements of different industries yet[6,7]. Usually, the alloying and hot deformation methods are used to improve the mechanical properties of magnesium alloys. Currently, more rare earth (RE) elements, such as Y, Ce, Gd, and Nd, are added into magnesium alloys[8-10] to refine the grains, improve structure uniformity, and form a high-strength secondary phase, thereby improving the comprehensive mechanical properties of magnesium alloys[11-13]. The deformed Mg-Zn-Zr alloy has excellent mechanical properties, compared with the

common Mg-Al-Zn alloys, such as AZ31 and AZ91 alloys, and the mechanical properties of ZK60 magnesium alloy can be further improved by adding RE elements[14]. Zhou et al[15] studied the effects of sole addition of Nd and combined addition of Nd and Y on the structure and mechanical properties of Mg-6Zn-0.5Zr alloy. It is found that the addition of Nd and Y refines the grains of the as-cast and as-extruded structures, hence improving the mechanical properties. Zengin et al[16] studied the structure and corrosion properties of Mg-Zn-Y-Nd-Zr alloys, and reported that with the addition of RE element, the dynamic recrystallization (DRX) grain size of as-extruded alloy is decreased, and DRX ratio is increased. The average DRX grain size and ratio are increased with increasing the extrusion temperature. Lv et al[17] reported that after adding 1.5wt% Nd into Mg-6.0Zn-0.5Zr alloy, two Mg-Zn-Nd ternary phases are formed: W phase and T phase. Adding Nd can significantly refine DRX grains, and the yield strength of alloy can reach 400 MPa. Qiu et al[18] reported that

the Mg-6Zn-1.5Nd-0.5Zr bar extruded at a relatively low temperature of 290 °C has excellent mechanical properties. Its yield strength exceeds 400 MPa, and the ultimate tensile strength exceeds 420 MPa.

In this research, the effects of Nd addition on the microstructure, mechanical properties, and DRX texture of Mg-Zn-Y-Zr alloys were studied.

## 1 Experiment

The Mg-6Zn-Y-$x$Nd-0.5Zr alloys with $x$=0, 0.5, 1.0 (wt%) were prepared by the smelting method, and are regarded as Alloy I, Alloy II, and Alloy III, respectively. The alloys were synthesized with pure Mg (99.98wt%), pure Zn (99.97wt%), Mg-30wt% Y, Mg-30wt% Nd, and Mg-30wt% Zr master alloys as starting materials in vacuum melting furnace under the protective atmosphere of $CO_2$ and $SF_6$ with the ratio of 99:1. The melt was poured into a cylindrical steel mold with the diameter of 120 mm, which was preheated to 300 °C. Then the melt was stored at 720 °C for 20 min and then water-cooled to form the as-cast ingot with the diameter of 120 mm and the height of about 100 mm. The actual chemical composition of the molten alloy was measured by inductively coupled plasma (ICP), as shown in Table 1. The ingot was homogenized at 400 °C for 12 h to reduce the segregation and casting defects, and then extruded into a bar with the diameter of 25 mm at 390 °C. The extrusion ratio was 10:1. After extrusion, the alloy was peak-aged at 180 °C for 60 h.

The phase analysis of the as-cast alloys was conducted through X-ray diffractometer (XRD, Rigaku D/MAX-2500PC). The scanning angle of the copper target was 10°~90°, and the scanning speed was 2°/min. Optical microscope (OM), scanning electron microscope (SEM, TESCAN Vega II Lum), and transmission electron microscope (TEM, FEI TECNAI G2 F20) were used to observe the microstructures under the accelerating voltage of 200 kV. The electron backscattered diffractometer (EBSD, JEOL JSM-7800F, HKLChannel 5 system) was used to study the DRX microstructures of the alloys. The specimens for EBSD analysis were prepared by mechanical grinding, and then electropolished with AC2 electrolyte. The tensile tests were conducted by CMT-5105 material testing machine, and the tensile direction was parallel to the extrusion direction (ED).

## 2 Results and Discussion

### 2.1 Microstructure of as-cast and as-extruded alloys

Fig. 1 presents XRD patterns of the as-cast Mg-Zn-$x$Nd-Zr alloys. Alloy I without Nd addition exhibits diffraction peaks corresponding to $\alpha$-Mg and W phase ($Mg_3Zn_3Y_2$). With increasing the Nd addition, the intensity of diffraction peaks
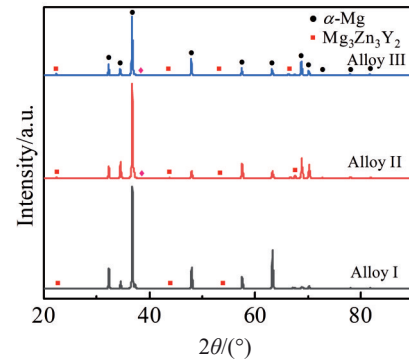


Fig.1　XRD patterns of as-cast Mg-6Zn-1Y-$x$Nd-0.5Zr alloys

of W phase is gradually increased.

OM microstructures and the grain size distributions of the as-cast alloys are shown in Fig. 2. The as-cast structure of Alloy I consists of relatively uniform equiaxed $\alpha$-Mg grains and some secondary phase particles, which are mainly distributed along the grain boundaries. With increasing the Nd content, the average grain size ($d$) of the as-cast alloys is gradually decreased. The average grain sizes of Alloy I, II, and III are about 68.0, 62.8, and 58.0 μm, respectively. The grain refinement effect is mainly due to the enrichment of Nd atoms in front of the solid-liquid interface during the solidification process. The increase in Nd atoms on the solid-liquid interface leads to the expansion of the supercooling zone, thereby accelerating the nucleation rate[19].

Fig.3 shows SEM microstructures of the as-cast alloys. The crystal grains become smaller and the amount of the secondary phase distributed along the grain boundary is gradually increased with the addition of Nd element. The secondary phase presents a discontinuous network distribution in Alloy I, and it gradually changes into the continuous full network distribution with increasing the Nd addition. The secondary phase accounts for 2.8%, 3.8%, and 5.7% in Alloy I, Alloy II, and Alloy III, respectively. The energy disperse spectroscopy (EDS) analyses show that the secondary phase in Alloy I is mainly composed of Mg, Zn, and Y, which corresponds to the $Mg_3Zn_3Y_2$ phase; the secondary phase in Alloy II and Alloy III is the $Mg_3Zn_3(Y, Nd)_2$ phase, indicating that the addition of Nd elements can partially replace the Y atoms[20].

OM microstructures of the Mg-6Zn-1Y-$x$Nd-0.5Zr alloys extruded at 390 °C are shown in Fig.4. It can be seen that the alloys undergo incomplete DRX during the hot extrusion process. The alloy structure is a typical bimodal structure consisting of recrystallized grains and deformed coarse unrecrystallized grains. In addition, a small amount of black secondary phase is distributed in the recrystallization zone. The longitudinal section parallel to ED and the cross-section perpendicular to ED are different, because the flow stress direction in the cross-section of the alloy bar is inconsistent during the extrusion process.

SEM microstructures of the extruded Mg-6Zn-1Y-$x$Nd-

Table 1　Chemical composition of Mg-Zn-Y-$x$Nd-Zr alloys (wt%)

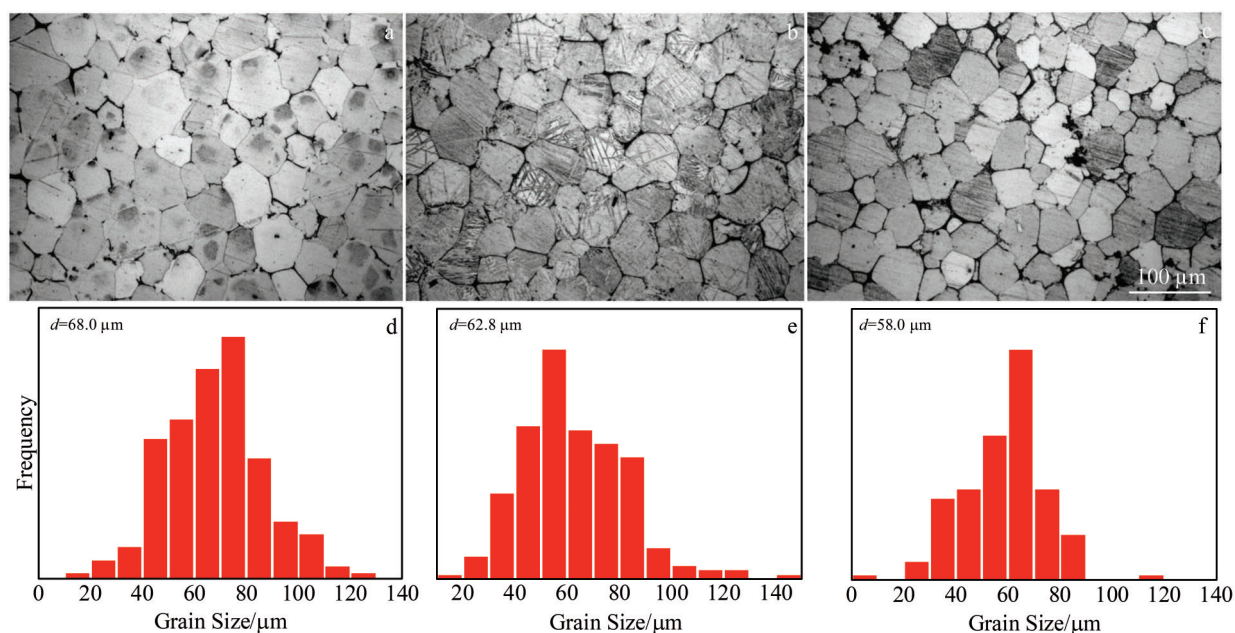| Alloy | Zn | Y | Nd | Zr | Mg |
|-------|------|------|------|------|------|
| I | 5.90 | 1.21 | 0.00 | 0.44 | Bal. |
| II | 6.42 | 1.04 | 0.64 | 0.47 | Bal. |
| III | 6.53 | 0.93 | 1.22 | 0.50 | Bal. |

Fig.2    OM microstructures (a~c) and grain size distributions (d~f) of as-cast Mg-6Zn-Y-*x*Nd-0.5Zr alloys: (a, d) Alloy I, (b, e) Alloy II, and (c, f) Alloy III
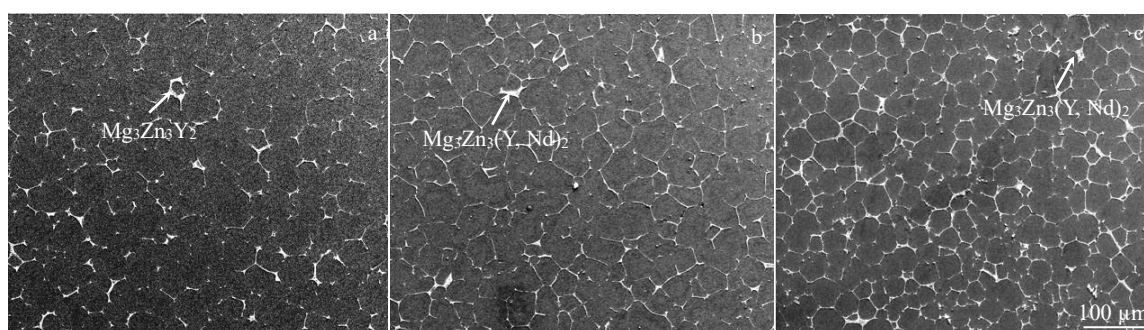


Fig.3    SEM microstructures of as-cast Mg-6Zn-1Y-*x*Nd-0.5Zr alloys: (a) Alloy I, (b) Alloy II, and (c) Alloy III

0.5Zr alloys are shown in Fig.5. The secondary phase particles are broken during the extrusion process and precipitated along ED. In addition, the secondary phases account for 4.4%, 4.6%, and 8.7% in the Alloy I, Alloy II, and Alloy III, respectively, indicating that the secondary phase is increased with increasing the Nd addition. EDS analysis results of the secondary phase in the as-extruded Mg-6Zn-1Y-*x*Nd-0.5Zr alloys are similar to those in the as-cast alloys. The secondary phase of Alloy I is $Mg_3Zn_3Y_2$ phase, and the secondary phase of Alloy II and Alloy III is $Mg_3Zn_3(Y, Nd)_2$ phase. The Nd element can hardly form the secondary phase alone, so it partially replaces the Y element in $Mg_3Zn_3Y_2$ phase, thereby forming the new secondary phase $Mg_3Zn_3(Y, Nd)_2$. The higher the Nd content, the larger the proportion of Nd element in the $Mg_3Zn_3(Y, Nd)_2$ phase.

The bright field TEM image of the secondary phase in as-extruded Alloy II is shown in Fig. 6a. It can be seen that different secondary phases with different sizes and morphologies are distributed in the as-extruded alloy. Three points (A, B, C) were selected for EDS analyses in Fig. 6b.

The high-angle annular dark field-scanning transmission electron microscope (HAADF-STEM) was used for analysis. The secondary phase at point A mainly contains Mg, Zn, and Zr; the secondary phase at point B contains Mg, Zn, Zr, and a small amount of Y; the secondary phase at point C contains Mg, Zn, Y, and Nd. As shown in Fig. 6b, point B and C represent different secondary phase particles, and they are partially overlapped. It can be concluded that the secondary phases at point A and B mainly contain Zn and a small amount of Zr, and Y and Nd barely exist. Therefore, the secondary phases at point A and B is the $Zn_2Zr$ phase. The secondary phase at point C is the $Mg_3Zn_3(Y, Nd)_2$ phase, and the finer precipitates with smaller size are $\beta 1$ phase[21].

The bright field TEM images of the $Mg_3Zn_3(Y, Nd)_2$ phase in as-extruded Alloy II are shown in Fig.7. The inset in Fig.7a shows the selected area electron diffraction (SAED) pattern of the particle marked in Fig.7a. The particle is identified as the $Mg_3Zn_3(Y, Nd)_2$ phase with a special face-centered cubic structure. It can be seen that many nano-scale precipitates exist in the extruded Alloy II, which can be considered as the
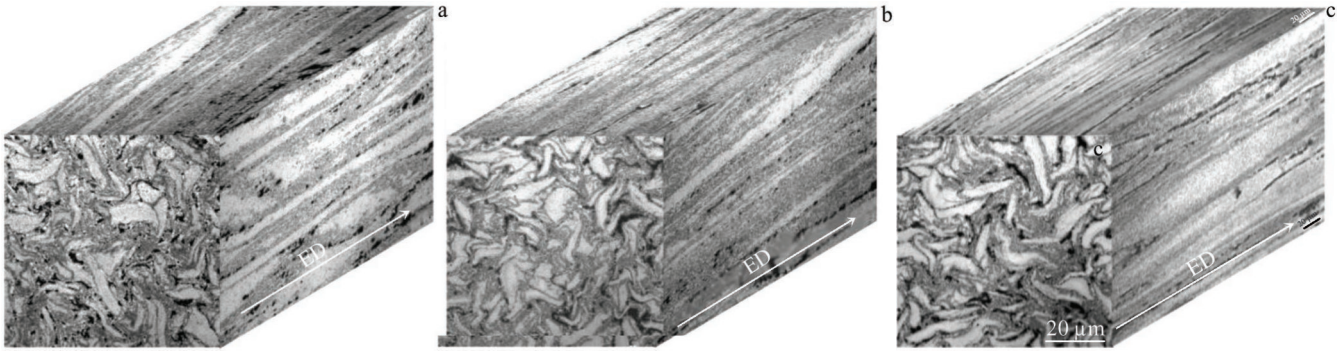
Fig.4    OM microstructures of as-extruded Mg-6Zn-Y-*x*Nd-0.5Zr alloys: (a) Alloy I, (b) Alloy II, and (c) Alloy III
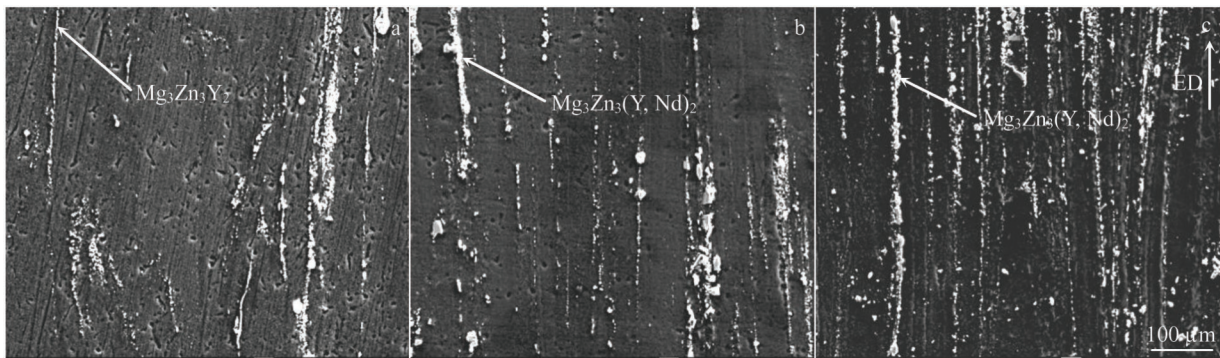


Fig.5    SEM microstructures of as-extruded Mg-6Zn-Y-*x*Nd-0.5Zr alloys: (a) Alloy I, (b) Alloy II, and (c) Alloy III
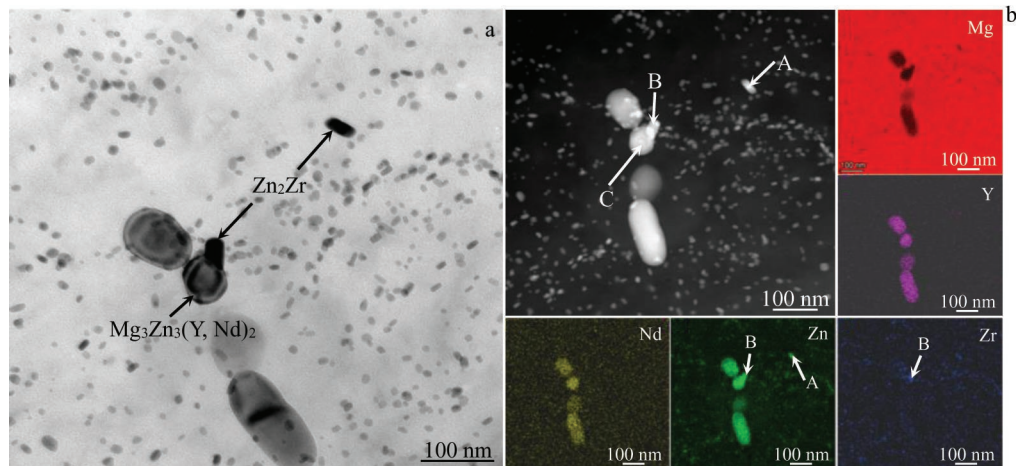


Fig.6    Bright field TEM image of as-extruded Alloy II (a); HAADF-STEM image and corresponding EDS element distributions of as-extruded Alloy II (b)

strengthening phase.

## 2.2    DRX and texture of as-extruded alloys

Fig. 8 shows the inverse pole figures (IPFs) of the as-extruded Mg-6Zn-Y-*x*Nd-0.5Zr alloys and the grain size distributions of DRX grains. The average DRX grain size of Alloy I, Alloy II, and Alloy III is 1.9, 1.7, and 1.4 μm, respectively. It can be seen that the coarse and elongated unDRX grains mainly show the basal plane orientation, while the orientation of the fine DRX grains is more random. The

unDRX area fraction accounts for 67%, 33%, and 47% in the Alloy I, Alloy II, and Alloy III, respectively, indicating that the Nd addition promotes DRX and grain refinement.

The $(10\bar{1}0)$ pole figures of the as-extruded Mg-6Zn-Y-*x*Nd-0.5Zr alloys are shown in Fig. 9. It can be seen that the extruded textures of the three alloys are basically the same, i.e., they are all typical $<10\bar{1}0>$ extruded wire textures. The maximum texture intensity in the pole figures all appears on the $(10\bar{1}0)$ plane, which is 37.0, 24.4, and 22.4 for the Alloy I,
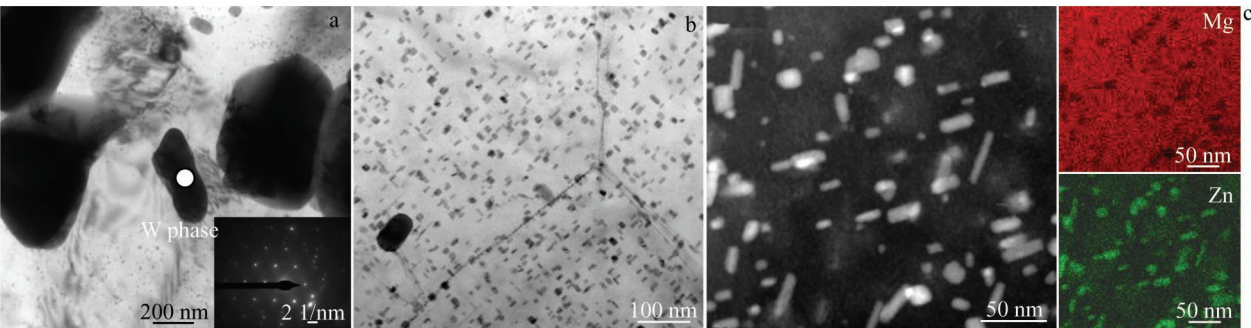
Fig.7   Bright field TEM images of $Mg_3Zn_3(Y, Nd)_2$ phase and SAED pattern of the marked particle (a) and fine precipitates (b) in as-extruded Alloy II; TEM image and corresponding EDS element distributions of as-extruded Alloy II (c)
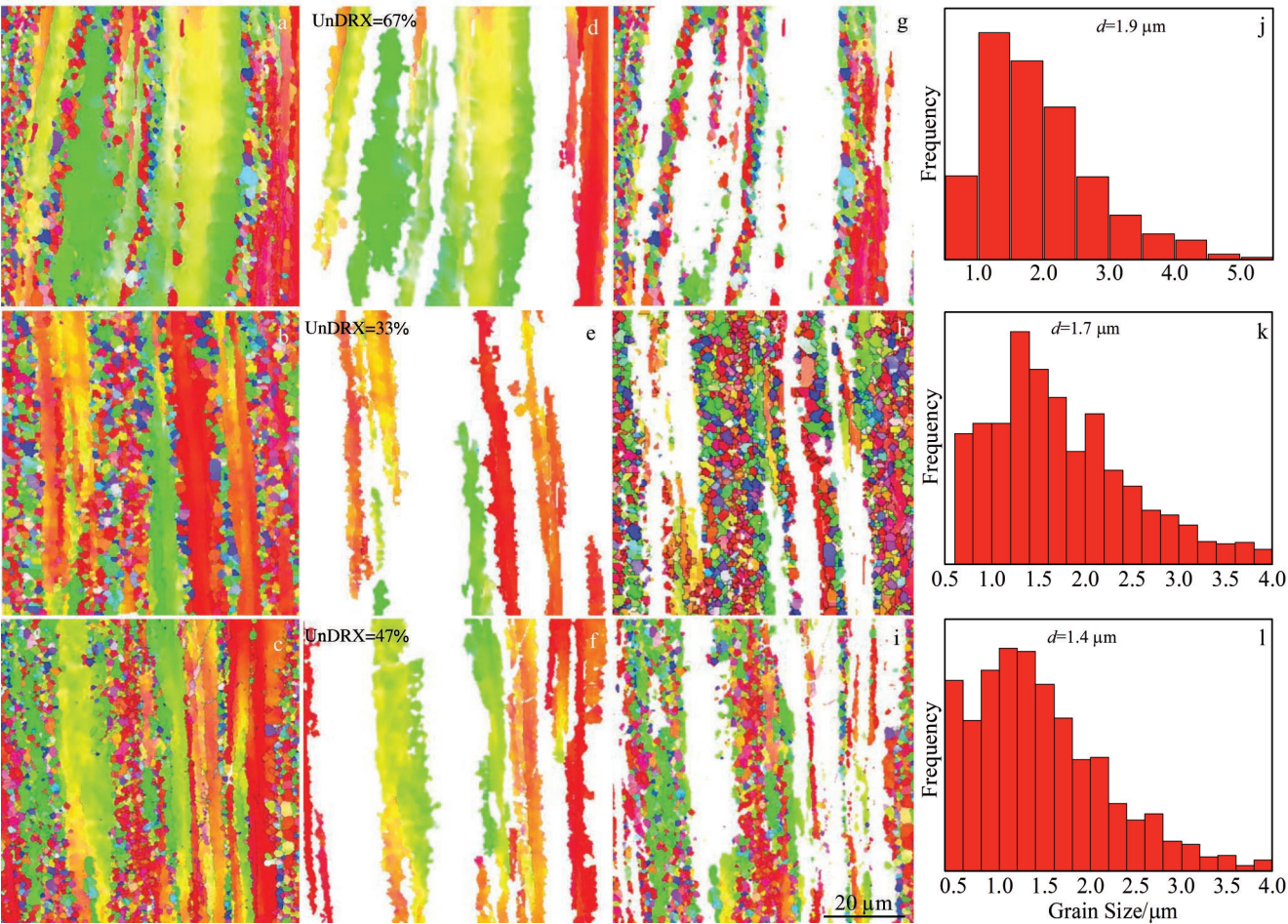


Fig.8   IPFs of overall (a~c), unDRX (d~f), and DRX (g~i) areas of as-extruded Alloy I (a, d, g), Alloy II (b, e, h), and Alloy III (c, f, i); DRX grain size distributions of Alloy I (j), Alloy II (k), and Alloy III (l)

Alloy II, and Alloy III, respectively. Therefore, the Nd addition weakens the texture strength of the alloys. With increasing the Nd content, the texture strength of the alloy is decreased. It is also found that the overall textures, DRX textures, and unDRX textures are basically the same, presenting the basal orientation textures with different texture intensities. For Alloy II, the texture intensity of the overall organization, DRX zone, and unDRX zone is 24.4, 11.8, and

46.3, respectively. The unDRX grains suffer violent plastic deformation during the hot extrusion process and show a strong basal plane orientation accompanied by slip and twinning. Because of DRX grains, the orientation of the newly formed recrystallized grains is relatively random, thereby weakening the texture in DRX zone. After the newly recrystallized grains are formed, they still suffer a small amount of plastic deformation, and therefore the weak basal
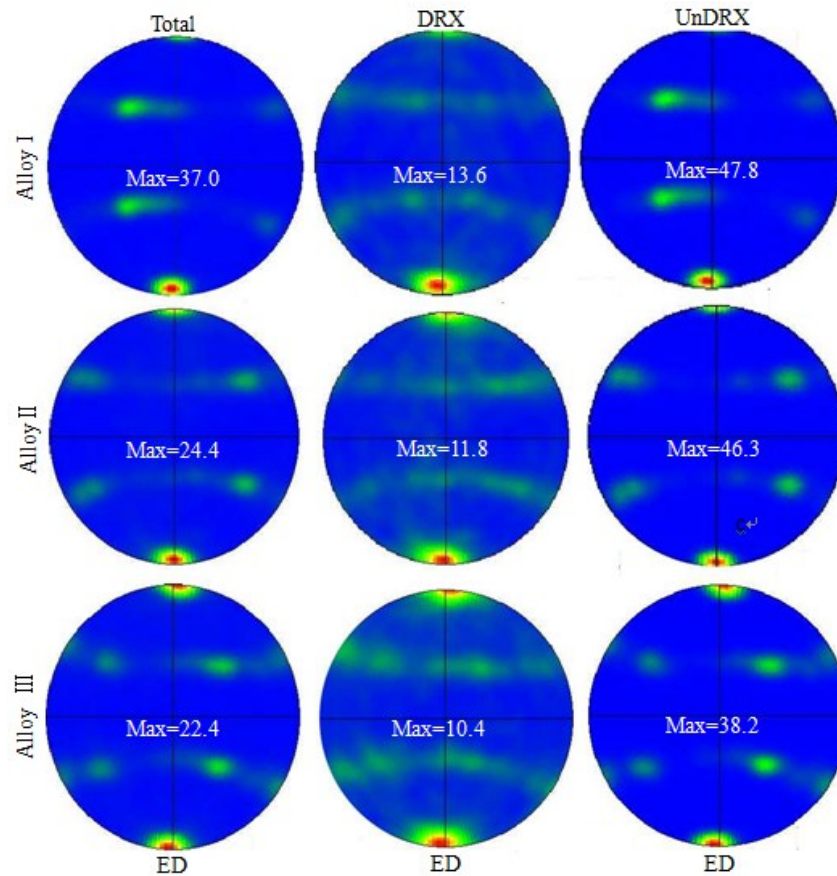
Fig.9    (100) pole figures measured by EBSD for as-extruded Mg-6Zn-Y-*x*Nd-0.5Zr alloys

surface texture appears. The similar results can be obtained in the DRX and unDRX zones of Alloy I and Alloy III. The unDRX region presents the strongest basal texture and the DRX region presents the weak texture.

The related texture parameters are shown in Table 2. Because the overall texture is composed of DRX and unDRX regions, the overall texture strength is affected by the combined intensity of DRX and unDRX textures. It is found that the theoretical maximum pole intensity is closer to the measured one. Therefore, it is believed that the texture intensity of the extruded bimodal structure is closely related to the DRX texture intensity, unDRX texture intensity, and DRX ratio.

Fig. 10 shows the (0002) and ($10\overline{1}0$) macro-textures of the Mg-6Zn-Y-*x*Nd-0.5Zr alloys. It can be seen that the macro- and micro-textures are basically the same and the texture intensity is gradually decreased with increasing the Nd addtion. The Nd addition weakens the overall texture of the

alloys by promoting DRX. It can be seen that with the Nd addition, the grains are refined, the proportion of the secondary phase is increased, and DRX ratio is increased, while the area of unrecrystallized grains is reduced and the texture is weakened. Because the secondary phase is evenly distributed in DRX area, according to the particle simulated nucleation mechanism, the secondary phase of a certain size can be used as the nucleation site for DRX. Therefore, it can be inferred that the Nd addition leads to the formation of more secondary phases, which can serve as new DRX nucleation sites and then promote DRX[22]. When more DRX grains with random orientation are generated, the overall texture of the alloy is weakened.

## 2.3 Mechanical properties of as-extruded and peak-aged alloys

Fig. 11 shows the engineering stress-engineering strain curves of as-extruded and peak-aged alloys, and the tensile properties are shown in Table 3. The as-extruded Alloy II with

Table 2    Texture parameters of as-extruded Mg-6Zn-Y-*x*Nd-0.5Zr alloys

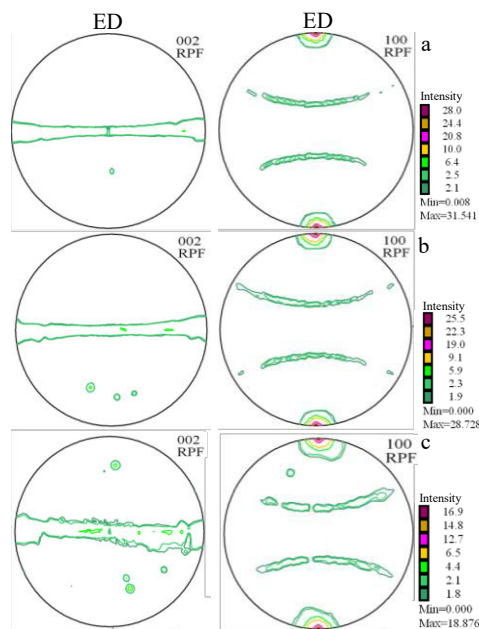| Alloy | DRX maximum texture intensity | DRX area fraction/% | UnDRX maximum texture intensity | UnDRX area fraction/% | Theoretical texture maximum intensity | Measured texture maximum intensity |
|---|---|---|---|---|---|---|
| I | 13.6 | 33 | 47.8 | 67 | 36.5 | 37.0 |
| II | 11.8 | 67 | 46.3 | 33 | 23.2 | 24.4 |
| III | 10.4 | 53 | 38.2 | 47 | 23.4 | 22.4 |

Fig.10 (0002) and (10$\bar{1}$0) macro-textures of as-extruded Alloy I (a), Alloy II (b), and Alloy III (c)

0.5wt% Nd has the optimal mechanical properties: the yield strength is 362 MPa, the ultimate tensile strength is 404 MPa, and the elongation is 10.2%. Therefore, the Nd addition can obviously improve the mechanical properties of Mg-Zn-Y-Zr alloys. When 1wt% Nd is added into the alloy, the mechanical properties of Alloy III are more inferior to those of Alloy II, which may be attributed to the coarsening of the secondary phase.

The Nd addition can refine the grains of the as-extruded alloys. According to Hall-Petch formula[23], the yield strength is inversely proportional to the grain size. The grain refinement can simultaneously improve the strength and plasticity of the alloys, because the internal dislocations and stress concentrations within the grains are less and greater external force is required to cause plastic deformation due to the existence of fine grains. Besides, the Nd addition leads to the formation of more Mg-Zn-RE phases, and a large number of nano-scale precipitates are precipitated during the hot extrusion process. These fine and dispersed secondary phase particles interact with the dislocations during the deformation process to hinder the dislocation movement[24], thereby improving the alloy rigidity, namely the dispersion
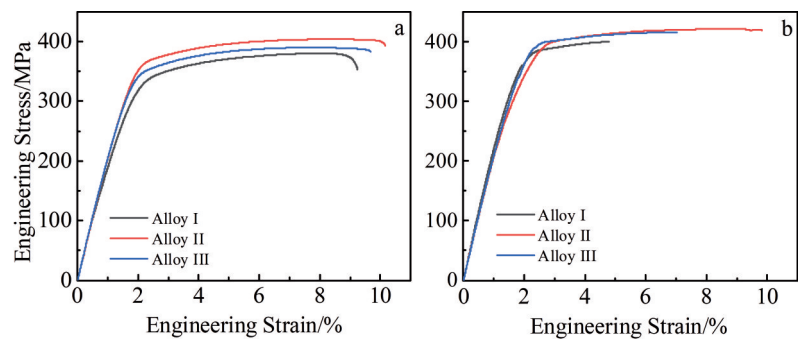


Fig.11 Engineering stress-engineering strain curves of as-extruded (a) and peak-aged (b) Mg-6Zn-Y-$x$Nd-0.5Zr alloys

**Table 3 Mechanical properties of as-extruded and peak-aged Mg-6Zn-Y-$x$Nd-0.5Zr alloys at room temperature**

| Alloy | Process | Yield strength/MPa | Ultimate tensile strength/MPa | Elongation/% |
|-------|---------|--------------------|--------------------------------|--------------|
| I | Hot extrusion | 337 | 380 | 9.2 |
| | Hot extrusion+T5 peak aging | 359 | 400 | 4.8 |
| II | Hot extrusion | 362 | 404 | 10.2 |
| | Hot extrusion+T5 peak aging | 386 | 421 | 9.8 |
| III | Hot extrusion | 346 | 390 | 9.7 |
| | Hot extrusion+T5 peak aging | 385 | 415 | 7.0 |

strengthening. In addition, with the Nd addition, the alloy texture is weakened and the plasticity is increased. These influence factors jointly affect the mechanical properties of the Mg-Zn-Y-Zr alloys.

After peak-aging treatment, the yield strength and tensile strength are further improved, while the plasticity is reduced. This phenomenon shows the strengthening effect caused by the precipitation of a large number of fine nano-scale secondary phases. For the peak-aged alloys, Alloy II still

presents the optimal mechanical properties: the yield strength is 386 MPa, the ultimate tensile strength is 421 MPa, and the elongation is 9.8%. Compared with those of the as-extruded alloys, the mechanical properties are significantly improved, and the plasticity is slightly decreased, which is attributed to the reduction in defects after aging treatments.

## 3 Conclusions

1) The Nd addition partially replaces the Y atoms of the

secondary phase $Mg_3Zn_3Y_2$ in Mg-6Zn-1Y-0.5Zr alloys, forming the new W phase $Mg_3Zn_3(Y, Nd)_2$ without changes in crystal structure.

2) Incomplete dynamic recrystallization occurs during the hot extrusion process. The Mg-Zn-rare earth phase generated by the Nd addition can be used as the nucleation site for dynamic recrystallization, thereby promoting the dynamic recrystallization. More recrystallized grains with random orientations are generated, thus weakening the texture of the alloys.

3) The peak-aged Mg-6Zn-1Y-0.5Nd-0.5Zr alloy presents the optimal mechanical properties: the yield strength is 386 MPa, the ultimate tensile strength is 421 MPa, and the elongation is 9.8%.

## References

1 Chen X H, Pan F S, Mao J J *et al. Materials & Design*[J], 2011, 32(3): 1526

2 Liu C Q, Chen X H, Chen J *et al. Journal of Magnesium and Alloys*[J], 2021, 9(3): 1084

3 Liu C Q, Chen X H, Yuan Y *et al. Journal of Materials Science & Technology*[J], 2021, 78: 20

4 Liu L Z, Chen X H, Pan F S *et al. Journal of Alloys and Compounds*[J], 2016, 688(B): 537

5 Yang Y, Xiong X M, Chen J *et al. Journal of Magnesium and Alloys*[J], 2021, 9(3): 705

6 Peng F, Zhang D D, Liu X Y *et al. Journal of Magnesium and Alloys*[J], 2021, 9(5): 1741

7 Zhao C Y, Chen X H, Pan F S *et al. Journal of Materials Science & Technology*[J], 2019, 35(1): 142

8 Wei X X, Jin L, Wang F H *et al. Journal of Materials Science & Technology*[J], 2020, 44: 19

9 Yu Z J, Huang Y D, Qiu X *et al. Materials Science and Engineering A*[J], 2015, 622: 121

10 Zhang D D, Yang Q, Guan K *et al. Journal of Alloys and Compounds*[J], 2019, 810: 151 967

11 Du B N, Hu Z Y, Sheng L Y *et al. Journal of Materials Science & Technology*[J], 2021, 60: 44

12 Xu S W, Zheng M Y, Kamado S *et al. Materials Science and Engineering A*[J], 2011, 528(12): 4055

13 Yamasaki M, Hashimoto K, Hagihara K *et al. Acta Materialia* [J], 2011, 59(9): 3646

14 Robson J D, Paa-Rai C. *Acta Materialia*[J], 2015, 95: 10

15 Zhou H T, Zhang Z D, Liu C M *et al. Materials Science and Engineering A*[J], 2007, 445-446: 1

16 Zengin H, Turen Y. *Journal of Magnesium and Alloys*[J], 2020, 8(3): 640

17 Lv S H, Meng F Z, Lu X L *et al. Journal of Alloys and Compounds*[J], 2019, 806: 1166

18 Qiu Xin, Yang Qiang, Cao Zhanyi *et al. Rare Metals*[J], 2016, 35(11): 841

19 Du Y Z, Qiao X G, Zheng M Y *et al. Materials Science and Engineering A*[J], 2015, 620: 164

20 Gong Z W, Wang J F, Sun Y F *et al. Materials Today Communications*[J], 2021, 27: 102 308

21 Rosalie J M, Somekawa H, Singh A *et al. Materials Science and Engineering A*[J], 2012, 539: 230

22 Jiang M G, Xu C, Yan H *et al. Acta Materialia*[J], 2018, 157: 53

23 Tu T, Chen X H, Zhang L J *et al. Rare Metal Materials and Engineering*[J], 2021, 50(2): 488

24 Hu H J. *Rare Metal Materials and Engineering*[J], 2021, 50(2): 416

# Mg-Zn-Y-Nd-Zr合金的显微组织、织构、力学性能

王子怡[1]，陈先华[1,2]，舒彦凯[1]，李建波[1]，袁　媛[1]，谭　军[1]，潘复生[1,2]

(1. 重庆大学 材料科学与工程学院，重庆　400045)
(2. 国家镁合金工程技术研究中心，重庆　400044)

**摘　要：** 对Mg-Zn-Y-Nd-Zr合金的显微组织和力学性能进行了研究。结果表明，Nd元素的加入部分取代了W相（$Mg_3Zn_3Y_2$）中的Y元素，形成了新的第二相$Mg_3Zn_3(Y, Nd)_2$。热挤压后观察到由细小的等轴再结晶晶粒和粗大的细长未再结晶晶粒组成的典型双峰结构。Nd元素的加入促进了热挤压过程中的动态再结晶，随着Nd含量的增加，动态再结晶率增加，挤压态合金的整体织构强度减弱。Nd的加入细化了晶粒并改善了合金的力学性能。添加0.5%（质量分数）Nd时，挤压态合金表现出高强度和高塑性的良好结合：屈服强度为362 MPa，极限抗拉伸强度为404 MPa，延伸率为10.2%。时效处理后合金的抗拉伸强度进一步提高，峰值时效极限抗拉强度可达421 MPa。合金的高强度主要归功于超细再结晶晶粒和析出强化。

**关键词：** Mg-Zn-Y-Nd-Zr合金；动态再结晶；力学性能；织构